

Solvable \mathcal{PT} -symmetric model with a tunable interspersion of non-merging levels.

Miloslav Znojil¹

Ústav jaderné fyziky AV ČR, 250 68 Řež, Czech Republic

Abstract

We study the spectrum in such a \mathcal{PT} -symmetric square well (of a diameter $L \leq \infty$) where the “strength of the non-Hermiticity” is controlled by the two parameters, viz., by an imaginary coupling ig and by the distance $\ell < L$ of its onset from the origin. We solve this problem and confirm that the spectrum is discrete and real in a non-empty interval of $g \leq g_0(\ell, L)$. Surprisingly, a specific distinction between the bound states is found in their asymptotic stability/instability with respect to an unlimited growth of g beyond $g_0(\ell, L)$. In our model, *all* of the low-lying levels remain asymptotically unstable at the small $\ell \approx 0$ and finite L while only the stable levels survive near $\ell \approx L < \infty$ or in the purely imaginary force limit with $0 < \ell < L = \infty$. In between these two extremes, an unusual classification of the interspersed levels is obtained.

PACS 03.65.Ge, 03.65.Ca, 02.30.Tb, 02.30.Hq
MSC 2000: 81Q05, 81Q10, 46C20, 47B50, 34L40

¹e-mail: znojil@ujf.cas.cz

1 Introduction

1.1 Non-Hermitian square-well-type models

Within the framework of \mathcal{PT} -symmetric Quantum Mechanics as formulated by Bender and Boettcher in 1998 [1], a one-parametric non-Hermitian square well (NSW) model has been described in ref. [2]. A key merit of the NSW model lies in a combination of its straightforward mathematical solvability with an exceptional transparency of its applications. In this way, the NSW model was able to offer an insight into the mechanism of the spontaneous \mathcal{PT} -symmetry breaking [3]. Next, due to its elementary character, the NSW model has been selected by Bagchi et al [4] as a starting point of a systematic supersymmetric generation of solvable non-Hermitian Hamiltonians with \mathcal{PT} -symmetry and real spectra. Last but not least, Mostafazadeh and Batal [5] choose the NSW model in their very recent illustrative application of the \mathcal{PT} -symmetric Quantum Mechanics in its present, mathematically as well as physically more or less consistent updated form (readers may consult some of the available reviews for more details [6]).

In our recent paper [7] we revealed that a certain “hidden” shortcoming of the NSW model may be seen in its “fragility”, i.e., in an instability of all the higher energy levels with respect to a certain highly speculative form of a complex-coordinate perturbation. Although such an observation does not have any *immediate* impact on the applications of the NSW model in refs. [3, 4, 5], certain doubts survive concerning the possible manifestations of some more serious instabilities in some of the generalized, NSW-type (NSWT) models.

For our present purposes let us vaguely characterize the latter NSWT potentials as piecewise constant. Then we may immediately recollect the existence of several “user-friendly” NSWT examples incorporating square-well models on a compact domain [8] or systems based on the use of point interactions [9]. Unfortunately, even within this class, the expectations concerning the stability of the spectrum are not always fulfilled. One may recollect, e.g., a spontaneous complexification of the high-lying part of many NSWT spectra as detected in very early numerical studies of certain particular potentials in ref. [10]. The phenomenon looks puzzling and makes all the NSWT models worth a more detailed non-numerical study.

1.2 The choice of a specific example

Within the framework of \mathcal{PT} -symmetric Quantum Mechanics we intend to pay attention to the family of Schrödinger equations

$$\left[-\frac{d^2}{dx^2} + V(x) + iW(x) \right] \psi(x) = E \psi(x) \quad (1)$$

(in units $\hbar = 2m = 1$) where the interaction is non-Hermitian but manifestly \mathcal{PT} -symmetric, i.e., where the real and imaginary parts of the potential are spatially symmetric and antisymmetric functions, respectively, $V(x) = +V(-x)$ and

$W(x) = -W(-x)$. For the sake of definiteness we shall contemplate the less interesting real part of the potential just in the most elementary infinitely deep square-well form,

$$V(x) = \begin{cases} +\infty \\ 0 \\ +\infty \end{cases} \quad \text{for} \quad \begin{cases} x > L \\ -L < x < L \\ x < -L. \end{cases} \quad (2)$$

This means that all our wave functions have to vanish at its walls,

$$\psi(-L) = \psi(L) = 0. \quad (3)$$

By adding any imaginary interaction we break the Hermiticity of the Hamiltonian. By doing so in the \mathcal{PT} -symmetric manner we preserve a chance and good hope of having the energies real [1].

For the sake of definiteness and in a way generalizing the NSW model of ref. [2] we shall assume that the Hermiticity-breaking term W is composed of two purely imaginary steps which both vanish inside a subinterval $(-\ell, \ell)$ of the interval $(-L, L)$,

$$W(x) = \begin{cases} +ig, \\ 0 \\ -ig \end{cases} \quad \text{for} \quad \begin{cases} \text{Re } x > \ell > 0, \\ \text{Re } x \in (-\ell, \ell), \\ \text{Re } x < -\ell. \end{cases} \quad (4)$$

A priori, the strength of the Hermiticity-violating imaginary force may be expected proportional to the coupling $g > 0$ and inversely proportional to $\ell < L$.

In applied quantum mechanics the construction of the majority of phenomenological models relies quite heavily on the correspondence principle which tries to connect each quantum model with its classical predecessor. In this context, \mathcal{PT} -symmetric Quantum Mechanics offers a weakening of this connection [11]. Unfortunately, as long as the operator of parity \mathcal{P} itself is indefinite, the formalism requires an explicit *additional* construction of a Hamiltonian-dependent positively definite metric $\eta > 0$ in Hilbert space. It is worth adding that, equivalently, one may also construct a quasi-parity \mathcal{Q} [12] or charge \mathcal{C} [13], both defined as a product $\eta\mathcal{P}$.

In this context the authors of ref. [5] emphasized that the application of the formalism to the particular NSW model proved facilitated by a perturbative connection between the NSW model and a Hermitian square well. Their construction of $\eta^{(NSW)}$ profited from the existence of a finite-dimensional matrix approximation of the non-Hermitian part of the NSW Hamiltonian. In this sense, a transition to the extended NSW class of models looks promising and motivates our present study.

Our interest in the particular two-parametric model (4) results from the obvious need of an enhancement of flexibility of its one-parametric NSW predecessor and also from the lasting possibility of its rigorous mathematical description by means of the efficient moving-lattice method of ref. [7] (reviewed also briefly in Appendix A below). Among additional purposes of the study of the similar NSW models one may list a search for reliable comparisons between different potentials revealing, hopefully, some new, unnoticed characteristic features of their spectra. One would like to understand, i.e., how the details of the shape of $W(x)$ could influence the

stability of the spectrum, or how one could control the domain of parameters where all the energies remain real.

Some of the NSWT studies have been motivated by their potential capacity of mimicking the properties of unsolvable models and, in particular, of one of the most popular \mathcal{PT} -symmetric toy interactions $W(x) = ix^3$ [14]. Some parallels are definitely there since in the latter unsolvable case the spectrum was proved real, non-negative and discrete [15]. Of course, there are always good reasons for an introduction of more parameters in NSW. Thus, the new freedom of a weakening of the non-Hermiticity by the choice of $\ell > 0$ might simulate analogies with the Bender's and Boettcher's generalized \mathcal{PT} -symmetric family $W(x) = -(ix)^{3-\mu}$ characterized by an abrupt change of its spectral properties at $\mu = 1$ and by the spontaneous complexification of all the sufficiently high-lying energies inside the interval $\mu \in (1, 2)$ of the shape-parameter [1].

The possibility of the latter correspondence passes an easy test at $\ell = 0$ and $L = \infty$ when the general solutions of our Schrödinger eq. (1) are mere exponentials at any real $g > 0$. Once we demand that they vanish in infinity we have

$$\psi(x) = \begin{cases} B_+ \exp(-\sigma x), & \sigma^2 = ig - E, \quad \mathcal{R}e\sigma > 0, \quad x \in (0, \infty), \\ B_- \exp(\sigma' x), & \sigma'^2 = -ig - E, \quad \mathcal{R}e\sigma' > 0, \quad x \in (-\infty, 0). \end{cases} \quad (5)$$

When $x \rightarrow 0^\pm$ the coincidence of the right and left limit of $\psi(x)$ itself specifies the normalization, $B_+ = B_-$, while the second matching rule $\psi'(0^+) = \psi'(0^-)$ implies that $\sigma = -\sigma'$, i.e., equation (5) has no solutions at $g > 0$. It is of no avail to admit that $\mathcal{R}e \sigma \rightarrow 0$ and $\mathcal{R}e \sigma' \rightarrow 0$ and to employ the scattering boundary conditions since, unless $g = 0$, the matching-compatible states remain always incompatible with our differential Schrödinger equation on a half-line.

We may conclude that both the discrete and continuous spectra are empty at $\ell = 0$ for $g > 0$ and $L = \infty$. This re-confirms our above expectations since the emptiness of the spectrum also characterizes the Bender's and Boettcher's toy interaction $W(x) = -(ix)^{3-\mu}$ at the Herbst's extreme shape parameter $\mu = 2$ [16]. At the same time, the spectrum abruptly ceases to be empty at $\mu < 2$ [1] as well as at $\ell > 0$ while $L = \infty$ (cf. the proof of this assertion as given in Appendix B below).

2 The method

2.1 Wave functions and their matching

As long as our potential is piecewise constant at $0 < \ell < L < \infty$ we may postulate

$$\psi(x) = \begin{cases} \psi_-(x) = B_- \sinh \kappa^*(L + x), & x \in (-L, -\ell), \\ \psi_0(x) = C \cos kx + iD \sin kx, & x \in (-\ell, \ell), \\ \psi_+(x) = B_+ \sinh \kappa(L - x), & x \in (\ell, L) \end{cases} \quad (6)$$

where $\kappa = s + it$, $E = k^2 = t^2 - s^2$, $g = 2st > 0$ and where s , t and k are assumed real and, for the sake of definiteness, positive. In the other words, we assume that within

a not yet specified non-empty domain of parameters g and ℓ the \mathcal{PT} symmetry of the wave functions remains unbroken. In the way proposed in ref. [2] we prescribe the phase,

$$\psi(x) = \text{real symmetric} + \text{imaginary antisymmetric}$$

and deduce that C and D are real. Next, we differentiate

$$\psi'(x) = \begin{cases} \psi'_-(x) = \kappa^* B_- \cosh \kappa^*(L+x), & x \in (-L, -\ell), \\ \psi'_0(x) = -kC \sin kx + ikD \cos kx, & x \in (-\ell, \ell), \\ \psi'_+(x) = -\kappa B_+ \cosh \kappa(L-x), & x \in (\ell, L), \end{cases}$$

and write down the following four matching conditions,

$$\begin{aligned} \psi_-(-\ell) &= \psi_0(-\ell), & \text{i.e.,} & & B_- \sinh \kappa^*(L-\ell) &= C \cos k\ell - iD \sin k\ell, \\ \psi'_-(-\ell) &= \psi'_0(-\ell), & \text{i.e.,} & & \kappa^* B_- \cosh \kappa^*(L-\ell) &= kC \sin k\ell + ikD \cos k\ell, \\ \psi_+(\ell) &= \psi_0(\ell), & \text{i.e.,} & & B_+ \sinh \kappa(L-\ell) &= C \cos k\ell + iD \sin k\ell, \\ \psi'_+(\ell) &= \psi'_0(\ell), & \text{i.e.,} & & -\kappa B_+ \cosh \kappa(L-\ell) &= -kC \sin k\ell + ikD \cos k\ell. \end{aligned}$$

Two of them define the (complex) values of B_{\pm} so that we are left with the pair of the matching constraints,

$$(kC \sin k\ell + ikD \cos k\ell) \sinh \kappa^*(L-\ell) = (C \cos k\ell - iD \sin k\ell) \kappa^* \cosh \kappa^*(L-\ell)$$

$$(kC \sin k\ell - ikD \cos k\ell) \sinh \kappa(L-\ell) = (C \cos k\ell + iD \sin k\ell) \kappa \cosh \kappa(L-\ell).$$

These two relations are complex conjugate of each other so that we have to consider just one of them, say,

$$\begin{aligned} (kC \sin k\ell - ikD \cos k\ell) \sinh(s+it)(L-\ell) &= \\ &= (C \cos k\ell + iD \sin k\ell) \kappa \cosh(s+it)(L-\ell). \end{aligned} \quad (7)$$

with $k \geq 0$.

2.2 Matching equations in the $\sigma - \tau - \varrho$ space

After we abbreviate $\sigma = s(L-\ell)$, $\tau = t(L-\ell)$ and $\varrho = k\ell$, equation (7) reads

$$\begin{aligned} \varrho(L-\ell) (C \sin \varrho - iD \cos \varrho) [\sinh \sigma \cos \tau + i \cosh \sigma \sin \tau] &= \\ = \ell(\sigma + i\tau) (C \cos \varrho + iD \sin \varrho) [\cosh \sigma \cos \tau + i \sinh \sigma \sin \tau]. \end{aligned} \quad (8)$$

We have to keep in mind that

$$\tau^2 = \sigma^2 + \frac{(L-\ell)^2}{\ell^2} \varrho^2$$

while the respective real and imaginary parts of eq. (8) have to be treated as independent equations

$$\varrho(L-\ell) (C \sin \varrho \sinh \sigma \cos \tau + D \cos \varrho \cosh \sigma \sin \tau) =$$

$$\begin{aligned}
&= \ell [\sigma (C \cos \varrho \cosh \sigma \cos \tau - D \sin \varrho \sinh \sigma \sin \tau) - \\
&\quad - \tau (C \cos \varrho \sinh \sigma \sin \tau + D \sin \varrho \cosh \sigma \cos \tau)] \quad (9)
\end{aligned}$$

and

$$\begin{aligned}
&\varrho (L - \ell) (C \sin \varrho \cosh \sigma \sin \tau - D \cos \varrho \sinh \sigma \cos \tau) = \\
&= \ell [\sigma (C \cos \varrho \sinh \sigma \sin \tau + D \sin \varrho \cosh \sigma \cos \tau) + \\
&\quad + \tau (C \cos \varrho \cosh \sigma \cos \tau - D \sin \varrho \sinh \sigma \sin \tau)] . \quad (10)
\end{aligned}$$

In the next step we notice that the latter equations form a linear algebraic homogeneous set for the two coefficients C and D . They possess a nontrivial solution if and only if the secular determinant \mathcal{D} vanishes. After we abbreviate $\Omega = \tan \varrho$ (= a quickly oscillating function of ϱ), $T = \tan \tau$ (= a quickly oscillating function of τ) and $\Sigma = \tanh \sigma$ (= a monotonous and bounded function of σ) we can evaluate \mathcal{D} . After a lengthy calculation the secular condition $\mathcal{D} = 0$ acquires the following compact form

$$X(\sigma) + Y(\tau) + F(R) [x(\sigma) + y(\tau)] = 0 \quad (11)$$

where

$$\begin{aligned}
X(\sigma) &= \frac{1 + \Sigma^2}{1 - \Sigma^2} \sigma^2 = \sigma^2 \cosh 2\sigma , \\
Y(\tau) &= \frac{1 - T^2}{1 + T^2} \tau^2 = \tau^2 \cos 2\tau , \\
x(\sigma) &= \frac{\Sigma}{1 - \Sigma^2} \sigma = \frac{1}{2} \sigma \sinh 2\sigma , \\
y(\tau) &= \frac{T}{1 + T^2} \tau = \frac{1}{2} \tau \sin 2\tau , \\
F(R) &= \frac{1 - \Omega^2}{\Omega} R = \frac{2R}{\tan 2\varrho} , \quad \varrho = \varrho(R) = \frac{\ell}{L - \ell} R .
\end{aligned}$$

We may re-scale our coupling $g = 2Z/(L - \ell)^2$ and conclude that our Z -independent secular equation (11),

$$\sin 2\varrho(R) [\sigma^2 \cosh 2\sigma + \tau^2 \cos 2\tau] + R \cos 2\varrho(R) [\sigma \sinh 2\sigma + \tau \sin 2\tau] = 0 \quad (12)$$

only has to be complemented by the two trivial constraints

$$\sigma \tau = Z , \quad \tau^2 - \sigma^2 = R^2 . \quad (13)$$

The triplets of roots R_n , σ_n and τ_n of this triplet of equations with $n = 0, 1, \dots$ define all the bound-state energies E_n by the elementary formula

$$E_n = \frac{1}{(L - \ell)^2} R_n^2 \equiv \frac{1}{(L - \ell)^2} (\tau_n^2 - \sigma_n^2) . \quad (14)$$

In an indirect check of the recipe we may recollect its $\ell \rightarrow 0$ (i.e., $\varrho \rightarrow 0$) limit and conclude that our present eq. (12) degenerates smoothly and correctly back to the known secular $\ell = 0$ equation {cf. eq. Nr. (9) in ref. [2]}.

2.3 Matching in the moving-lattice representation

The basic tool for a rigorous analysis of the form of the solutions of our matching constraints is the moving-lattice method of ref. [7] as reviewed in Appendix A below. Skipping the majority of details let us only note that for an analysis of this type, one of the recommended techniques seems to be the reduction of the problem to $\sigma - \tau$ plane. Preserving the definition of $\tau = \tau(N, t)$ of Appendix A and replacing the definition of $\sigma = \sigma(N, t)$ by another formula,

$$\sigma = \sigma(N, t, K, r) = \pi \times \sqrt{[N + t]^2 + \left[\frac{L - \ell}{2\ell} (K + r) \right]^2},$$

we eliminate the coordinate R . A shortcoming of this approach is that our matching condition (12) transferred into the $\sigma - \tau$ plane has to be understood as the following quadratic equation for τ ,

$$\Phi_t \tau^2 + \omega_{K,r,t} \tau + \Omega_{K,r,t}(\sigma) = 0 \quad (15)$$

where we abbreviated

$$\omega_{K,r,t} = \frac{(L - \ell) \pi \Psi_t}{2\ell \Xi_r} (K + r), \quad \Omega_{K,r,t}(\sigma) = \Xi_r \left[\sigma^2 \cosh 2\sigma + \frac{\omega_{K,r,t}}{\Psi_t} \sigma \sinh 2\sigma \right].$$

This defines $\tau = \tau_{K,r,t}(N)$ on the lattice, the ‘‘motion’’ of which will be controlled not only by t and r but also, not so strongly, by K . Technically, the price to be paid is still reasonable - we get the closed form of the matching-compatible function $\tau = \tau(\sigma)$ as the two well known root formulae from eq. (15). Nevertheless, significant simplifications of the resulting picture may be mediated by the direct inspection of the equations in question.

3 Solutions

3.1 Matching equations in the $\sigma - \tau$ plane

Building far-reaching analogies with the $\ell = 0$ special case would be misleading because the form of our matching constraint (12) is discontinuous in the limit $\ell \rightarrow 0$. Thus, let us assume that $\ell \neq 0$ and study eq. (12) in its full-fledged form. Firstly, we abbreviate $\mathcal{M}(\sigma, \tau) = \sigma \sinh 2\sigma + \tau \sin 2\tau$ and $\mathcal{N}(\sigma, \tau) = \sigma^2 \cosh 2\sigma + \tau^2 \cos 2\tau$ and re-write our matching constraint (12) as the secular equation

$$\mathcal{D}(\sigma, \tau, R) = Q(\sigma, \tau) + \frac{\tan 2\varrho(R)}{R} = 0, \quad Q(\sigma, \tau) = \frac{\mathcal{M}(\sigma, \tau)}{\mathcal{N}(\sigma, \tau)}. \quad (16)$$

This enables us to formulate several obvious observations.

- [O1] The shape of both the functions $\mathcal{M}(\sigma, \tau)$ and $\mathcal{N}(\sigma, \tau)$ of two variables is easily deduced using their separability, $\mathcal{X}(\sigma, \tau) = \mathcal{X}(\sigma, 0) + \mathcal{X}(0, \tau)$, $\mathcal{X} = \mathcal{M}, \mathcal{N}$.

[O2] The smoothness of the σ - and τ -dependence of the denominator $\mathcal{N}(\sigma, \tau)$ facilitates also the determination of the shape of $\mathcal{F}(\sigma, \tau) = 1/\mathcal{N}(\sigma, \tau)$.

[O3] In $\sigma - \tau$ plane we may visualize the shape of the second fraction in (16) as a function which is constant along hyperbolas $R(\sigma, \tau) = \sqrt{\tau^2 - \sigma^2} = \text{fixed}$.

All these innocent-looking observations have several far-reaching though not always obvious consequences and form in fact a background for a rigorous analysis of the spectrum.

3.2 A rigorous graphical interpretation of $Q(\sigma, \tau)$

In more detail, observation [O1] means that the surfaces defined by the two non-negative function(s) $\mathcal{X}(\sigma, 0) \geq 0$ have the form of the two only slightly different parabolic valleys with the same degenerate minimum (= zero) which coincides with the axis $\sigma = 0$. The pertaining second components $\mathcal{X}(0, \tau)$ differ more from each other but both are adding a structurally similar perpendicular set of infinitely many parallel hills and valleys possessing a steadily increasing (though always finite) amplitude. As an obvious result of the superposition, both the resulting surfaces $\mathcal{X}(\sigma, \tau)$ cross the zero plane merely along certain ovals $O_n^{\mathcal{X}}$, and both of them only get negative in their interior.

The precise shape of these ovals (numbered by $n = 0, 1, \dots$) may fully rigorously be determined using the moving-lattice method (cf. Appendix A) but even without any use of the moving lattices the qualitative character of their shape is obvious and we may conclude that the zero lines of $\mathcal{M}(\sigma, \tau)$ and $\mathcal{N}(\sigma, \tau)$ form the families of ovals $O_n^{\mathcal{M}}$ and $O_n^{\mathcal{N}}$ located within the stripes of $\tau \in [(n + 1/2)\pi, (n + 1)\pi]$ and $\tau \in [(n + 1/4)\pi, (n + 3/4)\pi]$, respectively. All of them are symmetric with respect to the reflection $\sigma \rightarrow -\sigma$ and their size in the σ direction increases with τ .

Examples of these structures may be found in both refs. [2] and [7] and another illustration appears in Figure 1 here. In fact, the Figure displays another surface $Q(\sigma, \tau) = \mathcal{M}(\sigma, \tau)/\mathcal{N}(\sigma, \tau)$ (within a narrow window of $0 \leq Q \leq 0.05$) but the shape of the curve where \mathcal{M} vanishes ($O_1^{\mathcal{M}} \equiv V_1$) appears there clearly since the denominator $\mathcal{F}(\sigma, \tau) = 1/\mathcal{N}(\sigma, \tau)$ has its zeros, generically, elsewhere (cf. observation [O2]). Besides the oval V_1 (and a part of $O_0^{\mathcal{M}} \equiv V_0$) the picture displays another oval $O_1^{\mathcal{N}} \equiv D_1$ of the zeros of the denominator \mathcal{N} . Incidentally it lies within the chosen interval of $\tau \in (3, 7)$ and remains visible due to a numerical artifact of a spurious projection of an infinite discontinuity of the function $\mathcal{F}(\sigma, \tau)$.

Although the visibility of the discontinuities reflects just an imperfection of the graphical representation of the surface, it will prove useful in what follows.

3.3 The role of the second component of $\mathcal{D}[\sigma, \tau, R(\sigma, \tau)]$

The presence of the subsurface generated by the second, R -dependent component $\mathcal{D}_{(R)}[R(\sigma, \tau)]$ in eq. (16) does not violate the separation between σ and τ too much (cf. observation [O3]). At the smallest absolute values of σ we may safely return to

the approximation of $\mathcal{D}_{(R)}[R(\sigma, \tau)]$ by a function of a single variable, $[\tan 2 \varrho(R)]/R \approx [\tan 2 \ell \tau / (L - \ell)]/\tau$. This picture only becomes deformed, at the larger σ , by being bent to the right, i.e., along hyperbolas $R(\sigma, \tau) = \text{constant}$.

A clear understanding of the τ -dependence of the whole surface $\mathcal{D}[\sigma, \tau, R(\sigma, \tau)]$ will be obtained when we distinguish between the domain of the “small τ ” {where $[\tan 2 \ell \tau / (L - \ell)]/\tau \approx 2 \ell / (L - \ell)$ is positive and virtually constant}, “medium τ ” {with the repeated quick growth of the curve $[\tan 2 \ell \tau / (L - \ell)]/\tau$ from minus infinity up to plus infinity within each interval of the constant length $\Delta \tau = \pi (L - \ell) / 2 \ell$ } and “large τ ” {where the values of $\mathcal{D}_{(R)}[R(\sigma, \tau)] \approx 1/\tau$ become very small up to the very thin layers near the singularity hyperbolas H_n }. Due to the local dominance of the latter singularities H_n at any $n = 0, 1, \dots$ it is easy to imagine that the sign of the whole function $\mathcal{D}[\sigma, \tau, R(\sigma, \tau)]$ is positive and negative in their left and right vicinity, respectively. This “rule of thumb” enables us to deduce the sign of the whole function $\mathcal{D}[\sigma, \tau, R(\sigma, \tau)]$ in all our Figures.

3.4 The left-moving hyperbolic discontinuities H_n

In the domain of the small shifts $\ell \ll 1$ the numerical values of the R -dependent component $\mathcal{D}_{(R)}[R(\sigma, \tau)]$ of eq. (16) remain almost constant and small. In this regime the above-mentioned “small- τ ” constraint $\tau \ll (L - \ell)/\ell$ is not particularly restrictive so that the matching-compatible roots of equation $\mathcal{D} = 0$ remain very similar to their $\ell = 0$ predecessors in quite a large leftmost portion of the $\sigma - \tau$ plane. In our notation, the first few ovals $O_n^{\mathcal{D}} \equiv V_n$ of the zeros of the secular determinant stay only perturbatively shifted and deformed by an increase of $\ell \ll 1$.

With the growth of ℓ or $\lambda = \ell / (L - \ell)$ the leftmost discontinuity-hyperbola H_0 of the surface $\mathcal{D}[\sigma, \tau, R(\sigma, \tau)]$ moves to the left and emerges in the right half of Figure 2 where we choose the scale-independent parameter $\lambda = 11/40$ which corresponds to $\ell = 11 L / 51$. This means that we are just leaving the domain of the small shifts $\ell \ll 1$ so that the deformation of the nodal oval $O_1^{\mathcal{D}} \equiv V_1$ becomes perceivable, caused by the closeness of H_0 to the ℓ -independent discontinuity oval $D_1 \equiv O_1^{\mathcal{N}}$ inherited from the never-vanishing factor $\mathcal{F}(\sigma, \tau) = 1/\mathcal{N}(\sigma, \tau)$.

In a way which generalizes the illustrative Figure 2, each hyperbolic singularity H_k (defined by the equation $R(\sigma, \tau) = (L - \ell)(k + 1/2)\pi/\ell$ with $k = 0, 1, \dots$) moves to the left with the growth of ℓ and λ . Once it gets close to the N -th singularity oval D_{N-1} , it touches it at a point with the coordinates $\sigma_{(in)}^{(N, k)} = 0$ and $\tau_{(in)}^{(N, k)} = (N - 1/4)\pi$ at the critical value $\lambda = 2\ell / (L - \ell) = (4k + 2)/(4N - 1) \equiv \lambda_{(in)}^{(N, k)}$ of the shift.

With the further growth of λ the intersection of the hyperbola with the standing oval moves to the left and disappears, curiously enough, at a certain pair of points with the “last-contact” $|\sigma| = |\sigma_{(out)}^{(N, k)}| > 0$ and $\tau = \tau_{(out)}^{(N, k)} < (N - 3/4)\pi$. The latter value lies slightly below the oval’s end. Let us skip here the proof of this subtlety as not too relevant.

3.5 A completion of the list of the nodal lines

We are now prepared to detect *all* the nodal curves of $\mathcal{D}[\sigma, \tau, R(\sigma, \tau)]$ and to determine their qualitative ℓ -dependence in all the interval of $\ell \in (0, L)$ and/or of $\lambda = \lambda(\ell) \in (0, \infty)$. For the first inspiration we return to Figure 2 where the oval of zeros $O_1^{\mathcal{D}} \equiv V_1$ cannot be interpreted as a mere small perturbation of $O_1^{\mathcal{M}}$ in spite of the fact that the singularity hyperbola H_0 still did not touch the singularity oval $O_1^{\mathcal{N}} \equiv D_1$ since $\lambda = 0.275 < \lambda_{(in)}^{(2,1)} = 2/7 \approx 0.286$.

Still, the much more important observation made in Figure 2 concerns the emergence of the new curve W_0 of the new zeros of the function \mathcal{D} . At the chosen λ this curve just entered Figure 2 at its right side. Our next Figure 3 confirms that the new nodal curve W_0 moves to the left and gets deformed in a way reflecting the presence of a steep oval dip in $Q(\sigma, \tau)$ below $\tau = 2\pi$. We choose $\lambda = 0.355$ which is still safely smaller than the lower estimate $(4k - 2)/(4N - 3) = 0.4$ of the singularity hyperbola's "jumped-over" parameter $\lambda_{(out)}^{(2,1)} \approx 0.403$.

The "next-step snapshot" of Figure 4 at $\lambda = 0.395$ shows how the same dip deforms the shape of the oval $O_1^{\mathcal{D}} \equiv V_1$ in the domain where the function of R is small. In the subsequent Figure 5 we finally see how the two curves of the zeros merge while a topologically new situation is created and sampled at $\lambda = 0.415 > \lambda_{(out)}^{(2,1)}$.

We may summarize that for the growing λ the motion of the singular component $\tan 2\varrho(R)/R$ of our secular determinant $\mathcal{D}(\sigma, \tau)$ to the left gives a clear guide how to keep the ℓ -dependence of its zero lines under full control. The emergence and the asymptotically hyperbolic shape of the new (and, in fact, not quite expected) non-oval curves W_m of zeros follows immediately from the asymptotic smallness of the positive component $Q(\sigma, \tau) \sim 1/\sigma^2$ of $\mathcal{D}(\sigma, \tau)$ at the larger $|\sigma| \gg 1$.

Due to the reasonably elementary character of the function $\mathcal{D}(\sigma, \tau)$ we are able to understand that the pattern sampled by the Figures 2 - 5 is entirely universal. Always, step by step, the nodal ovals V_n as well as their asymptotically hyperbolic nodal-line partners W_m become deformed by the existence of the dip in the numerator function $\mathcal{M}(\sigma, \tau)$.

Of course, after the hyperbola of singularities H_k as well as its strongly deformed trailing nodal curve W_k "creep" over the fixed singularity oval D_j (as well as over its attached and strongly deformed zero curve V_j), the smoother shapes of both the nodal curves W_k and V_j are more or less recovered, and only their ordering remains permanently reversed. In spite of the apparent nonlinearity of the "creeping-over" effects, their details might again be analyzed algebraically, using an adapted version of the moving-lattice method of section 2.3.

The most important reward compensating an increase in complexity of the latter recipe is that one becomes able to treat one of the two roots of eq. (15), say, as a "non-perturbative" solution at the small ℓ . The most important example of its role are the hyperbolic nodal curves W_m which move to the right in τ with the decrease of ℓ and which disappear in infinity in the NSW limit of $\ell \rightarrow 0$.

4 Energies

4.1 Graphical representation and classification

On the background of the preceding material, what remains for us to do is a combination of the above-described knowledge of the nodal lines of $\mathcal{D}[\sigma, \tau, R(\sigma, \tau)]$ with the coupling-dependence constraint $\sigma \times \tau = Z = (L - \ell)^2 g/2$. A sample of the intersections of this type (i.e., of a typical final solution) is offered in Figure 6 where $\lambda = 2.40$ is neither small nor large and where we choose $Z = Z^{(a)} = 1.00$ and $Z = Z^{(b)} = 2.24$ (= the critical “exceptional-point” value of ref. [2]) for illustration. The conclusions which are illustrated by this graph have a general validity:

- We always have $\tau > \sigma > 0$ which means that all the real bound-state energies E_n remain positive at $Z > 0$.
- Some of the energies remain real at *any* value of $Z > 0$. They correspond to the intersections of the hyperbola $\sigma = Z/\tau$ with the hyperbolic nodal lines W_m and may be called “stable”, $E = E_m^{(s)}$.
- All the other energies $E = E_n^{(u)}$ correspond to the intersections of the hyperbola $\sigma = Z/\tau$ with the nodal ovals V_k . At a sufficiently small Z the latter intersections remain real (see the line (a) with $Z = 1$ in Figure 6).
- We may call the latter energies “unstable” as they merge in pairs and form complex conjugate doublets [17] beyond certain “exceptional-point” [18] values of ℓ and Z (illustration: the line (b) in Figure 6).

The decomposition of the spectrum into its stable and unstable parts varies with ℓ or $\lambda = \ell/(L - \ell)$ in an obvious manner. Hence, the stability pattern in the spectrum will be entirely different at the small and large λ since in the former case the hyperbolic curves W_n only generate the high-lying energies and *vice versa*.

4.2 Numerical construction

After all our previous detailed analysis of the qualitative features of the spectrum the numerical determination of energies becomes fully routine. Indeed, as long as we know $\tau = Z/\sigma$, the rule $\tau^2 - \sigma^2 = R^2$ leads immediately to the definition of

$$\sigma = \sigma(R) = \sqrt{\frac{2 Z^2}{R^2 + \sqrt{R^4 + 4 Z^2}}}. \quad (17)$$

In parallel to such an introduction of the closed function $\sigma = \sigma(R)$ of R we may return once more to the recipe $\tau = Z/\sigma(R)$ and re-read it as another explicit definition of the second auxiliary function $\tau(R) = Z/\sigma(R)$ of R .

In such a setting, the purely numerical determination of the bound-state energies is reduced to the search for the roots R_n of eq. (12), i.e., of the zeros of the secular determinant

$$\hat{\mathcal{D}}(R) = \left[\sigma^2(R) \cosh 2 \sigma(R) + \tau^2(R) \cos 2 \tau(R) \right] \sin 2 \lambda R +$$

$$+R [\sigma(R) \sinh 2 \sigma(R) + \tau(R) \sin 2 \tau(R)] \cos 2 \lambda R \quad (18)$$

converted now in the function of the single variable $R \sim \sqrt{E}$. An illustration of such a search is given in Figure 7 at a fixed choice of $Z = 2$. The quadruplet of the graphs of the secular determinant $\hat{\mathcal{D}}(R) = \mathcal{D}[\sigma(R), \tau(R), R]$ is presented there at the four different values 1.25, 1.35, 1.45 and 1.55 of λ (indicated along the vertical axis). In each of these graphs we magnified the vertical units near $\hat{\mathcal{D}}(R) \approx 0$ and compressed them to a single point representing all the bigger values of $|\hat{\mathcal{D}}(R)| \geq \varepsilon$. In this way the picture samples the left-hand side of eq. (18) solely near its zeros. Our magnification of the vertical dimension marks these zeros by the virtually straight parts of the curve which are seen as practically perpendicular to the horizontal axis.

The set of graphs in Figure 7 illustrates the λ -dependence of the bound-state roots R_n . We see that a pair of the unstable energies may merge and cease to be real after a fine-tuned growth of λ . This illustrates the complexification of the unstable energies which is *not* caused by the growth of Z but rather by the growth of λ . At the first sight this phenomenon looks like a paradox because we are now *weakening* the non-Hermiticity in fact. Fortunately, this paradox is still easily understood once we imagine (and check, say, in the spirit of Figures 2 or 3) that the growth of λ “pushes” *all* the zeros (including of course also the nodal oval in question) to the left. Of course, this oval cannot get prolonged in the σ direction because the function $\mathcal{M}(\sigma, \tau)$ itself grows too quickly with σ . This implies that the two real intersections of the oval with the hyperbola $\sigma = Z/\tau$ disappear because the latter curve grows to the left.

In the light of an additional scaling in eq. (14) one may only admire the subtlety of the phenomenon, the verification of which very much profits from the exact solvability of the model. An independent confirmation of the absence of any contradictions may be also offered via a further simplification of mathematics. This inspires us to pay particular attention to the “most counterintuitive” limiting case where $L \rightarrow \infty$. Such an analysis may be of an independent interest as it simulates, very roughly, the shape of the most popular antisymmetric and purely imaginary potential $V(x) \sim i x^3$ with real spectrum [15]. As long as this discussion already lies somewhat beyond the scope the present text, it is moved to the Appendix B.

5 Conclusions

Recent progress in our understanding of the possible role of \mathcal{PT} -symmetric quantum Hamiltonians H in physics may be briefly summarized as an agreement that the role of the parity-type operator \mathcal{P} is just mathematical and auxiliary and that one must necessarily complement the model by a revitalization of its probabilistic tractability via an introduction of the “missing” standard metric $\eta = \mathcal{C}\mathcal{P}$. Similarly, one starts understanding the role of the time-reversal-type antilinear operator \mathcal{T} as merely mediating the Hermitian conjugation [17, 19]. We may conclude that during the last two or three years the \mathcal{PT} -symmetry lost its enigmatic character and has been accepted as just opening new horizons within the standard Quantum Mechanics [5, 20]. Hence, it is time for a deeper study of the simple and *tractable* models (like

the one presented here), keeping in mind the idea of their just emerging *consistent* phenomenological applicability, perhaps, in the nearest future.

In this context, an excitement caused by the reality of the spectra in many \mathcal{PT} -symmetric models has weakened its original impact. The emphasis of the research has been shifted, typically, to the explicit constructions of the charge \mathcal{C} [21] or to the more detailed analyses of what happens at the boundary points where the reality of the spectrum is being lost [18, 22]. A few unusual features exhibited by our present model seem to offer a clear and new intuitive guidance in this area.

The latter subject is interesting since the merger and subsequent spontaneous complexification of some “twin” pairs $E^{(\pm twin)}$ of the energies cannot be easily described within the usual textbook models where the metric is “trivial”, $\eta_{(trivial)} = I$. It is also in this context where considerations based on our present model could lead to a deeper insight in the underlying mechanisms and mathematics, not only because our model is solvable but also because it proves able to provide different “twin-merging” patterns in the spectrum. Indeed, by the choice of the shape parameter ℓ we may, up to a large extent, prescribe *which* particular excitations (say, in the low-lying spectrum) should remain robustly stable and which ones should form the unstable, fragile “twins” merging at some sufficiently large couplings $g_{(critical)}$.

In the similar constructions and studies, one might feel hesitant between the models which are simpler and the models which are more realistic. We believe that one should be able to transfer the insight gained in the solvable models (like in the present one) to all the more realistic applications where just some approximate methods can be used. In this sense we already mentioned a parallelism between the role of the shift ℓ in our solvable model and of the exponent μ in the power-law potentials with \mathcal{PT} -symmetry. In this comparison, our present model proves able to offer a much richer pattern of the mergers of the levels. It is only encouraging to see that a certain nontrivial enrichment of the merging pattern has been also detected, more or less in parallel, within the class of the power-law forces [22].

Acknowledgment

Partially supported by GA AS in Prague, contract No. A 1048302.

Figure captions

Figure 1. A thin slice through the surface $Q(\sigma, \tau) = \mathcal{M}/\mathcal{N}$.

Figure 2. A thin slice through the surface of the secular determinant $\mathcal{D}(\sigma, \tau)$ at $\lambda = \ell/(L - \ell) = 0.275$.

Figure 3. Same as Figure 2, $\lambda = 0.355$.

Figure 4. Same as Figure 2, $\lambda = 0.395$.

Figure 5. Same as Figure 2, $\lambda = 0.415$.

Figure 6. Solutions at $Z^{(a)} = 1.00$ and $Z^{(b)} = 2.24$, intersections marked by circles, $\lambda = 2.4$.

Figure 7. Four re-scaled graphs of the function $\hat{\mathcal{D}}(R)$.

Figure 8. Graphical solution of eq. (28) ($y = \omega_N/2, T = 1$)

References

- [1] C. M. Bender and S. Boettcher, Phys. Rev. Lett. 24 (1988) 5243.
- [2] M. Znojil, Phys. Lett. A. 285 (2001) 7.
- [3] M. Znojil and G. Lévai, Mod. Phys. Lett. A 16 (2001) 2273.
- [4] B. Bagchi, S. Mallik and C. Quesne, Mod. Phys. Lett. A17 (2002) 1651.
- [5] A. Mostafazadeh and A. Batal, Physical Aspects of Pseudo-Hermitian and PT -Symmetric Quantum Mechanics, preprint quant-ph/0408132
- [6] P. A. M. Dirac, Proc. Roy. Soc. London A 180 (1942) 1;
W. Pauli, Rev. Mod. Phys. 15 (1943) 175;
F. G. Scholtz, H. B. Geyer and F. J. W. Hahne, Ann. Phys. (NY) 213 (1992) 74,
M. Znojil, What is PT symmetry? preprint quant-ph/0103054v1, unpublished;
M. Znojil, Conservation of pseudo-norm in PT symmetric quantum mechanics, preprint math-ph/0104012, unpublished;
R. Kretschmer and L. Szymanowski, The Interpretation of Quantum-Mechanical Models with Non-Hermitian Hamiltonians and Real Spectra, preprint quant-ph/0105054, unpublished;
B. Bagchi, C. Quesne and M. Znojil, Mod. Phys. Letters A 16 (2001) 2047;
A. Mostafazadeh, J. Math. Phys. 43 (2002) 3944 and 6343.
B. Bagchi and C. Quesne, Phys. Lett. A 300 (2002) 18;
A. Ramírez and B. Mielnik, Rev. Fis. Mex. 49S2 (2003) 130;
Z. Ahmed and S. R. Jain, Phys. Rev. E 67 (2003) 045106(R);
A. Mostafazadeh, Czech. J. Phys. 53 (2003) 1079;
F. Kleefeld, in “Hadron Physics, Effective Theories of Low Energy QCD”, AIP Conf. Proc. 660 (2003) 325.
C. M. Bender, Czech. J. Phys. 54 (2004) 13.
- [7] M. Znojil, Fragile PT -symmetry in a solvable model, preprint math-ph/0403033, to appear in J. Math. Phys.
- [8] M. Znojil, J. Phys. A: Math. Gen. 36 (2003) 7825;
V. Jakubský, Czech. J. Phys. 54 (2004) 67;
V. Jakubský and M. Znojil, Czech. J. Phys. 54 (2004) 1101.
- [9] S. Albeverio, S. M. Fei and P. Kurasov, Lett. Math. Phys. 59 (2002) 227;
M. Znojil, J. Phys. A: Math. Gen. 36 (2003) 7639;
S. M. Fei, Czech. J. Phys. 54 (2004) 43.

- [10] C. M. Bender, S. Boettcher and P. N. Meisinger, *J. Math. Phys.* 40 (1999) 2201.
- [11] M. Znojil, *Czech. J. Phys.* 54 (2004) 151.
- [12] M. Znojil, *Phys. Lett. A* 259 (1999) 220 and 264 (1999) 108;
 G. Lévai and M. Znojil, *J. Phys. A: Math. Gen.*, 33 (2000) 7165;
 B. Bagchi, S. Mallik and C. Quesne, *Int. J. Mod. Phys. A* 17 (2002) 51;
 C. S. Jia, S. C. Li, Y. Li and L. T. Sun, *Phys. Lett. A* 300 (2002) 115;
 A. Sinha, G. Lévai and P. Roy, *Phys. Lett. A* 322 (2004) 78.
- [13] C. M. Bender, D. C. Brody and H. F. Jones, *Phys. Rev. Lett.* 89 (2002) 270401.
- [14] E. Caliceti, S. Graffi and M. Maioli, *Commun. Math. Phys.* 75 (1980) 51;
 G. Alvarez, *J. Phys. A: Math. Gen.* 27 (1995) 4589;
 E. Delabaere and D. T. Trinh, *J. Phys. A: Math. Gen.* 33 (2000) 8771;
 G. A. Mezincescu, *J. Phys. A: Math. Gen.* 33 (2000) 4911;
 C. R. Handy, *Czech. J. Phys.* 54 (2004) 57;
 M. Bentaiba, S. A. Yahiaoui and L. Chetouani, *Phys. Lett.* 231 (2004) 175.
- [15] P. Dorey, C. Dunning and R. Tateo, *J. Phys. A: Math. Gen.* 34 (2001) 5679;
 K. C. Shin, *Commun. Math. Phys.* 229 (2002) 543.
- [16] I. Herbst, *Commun. Math. Phys.* 64 (1979) 279.
- [17] A. Mostafazadeh, *J. Math. Phys.* 43 (2002) 205 and 2814.
- [18] C. Dembowski et al, *Phys. Rev. Lett.* 86 (2001) 787;
 W. D. Heiss and H. L. Harney, *Eur. Phys. J. D* 17 (2001) 149;
 U. Günther and F. Stefani, *J. Math. Phys.* 44 (2003) 3097;
 W. D. Heiss, *Czech. J. Phys.* 54 (2004), October issue, to appear.
- [19] A. Mostafazadeh, A Critique of PT-Symmetric Quantum Mechanics (arXiv: quant-ph/0310164, unpublished);
 C. M. Bender, D. C. Brody and H. F. Jones, *Phys. Rev. Lett.* 92 (2004) 119902 (erratum).
- [20] C. M. Bender, D. C. Brody and H. F. Jones, *Am. J. Phys.* 71 (2003) 1095;
 A. Mostafazadeh, *Czech. J. Phys.* 54 (2004), October issue, to appear (preprint quant-ph/0407213);
 M. Znojil, PT-symmetry, ghosts, supersymmetry and Klein-Gordon equation (arXiv: hep-th/0408081, unpublished).

- [21] C. M. Bender, Czech. J. Phys. 54 (2004), October issue, to appear;
E. Caliceti, F. Cannata, M. Znojil and A. Ventura, Construction of PT-asymmetric non-Hermitian Hamiltonians with CPT-symmetry (math-ph/0406031, submitted).
- [22] P. Dorey, A. Millican-Slater and R. Tateo, Beyond the WKB approximation in PT-symmetric quantum mechanics, hep-th/0410013.

Appendix A: The method of moving lattice

Secular eq. (12) and its descendants contain quickly oscillating trigonometric functions of arguments 2τ and 2ϱ . In the spirit of ref. [7] it makes sense to re-parametrize both these variables according to the rules

$$\tau = \tau(N, t) = \pi N + \pi t, \quad N = 0, 1, \dots, \quad t \in (0, 1),$$

$$\varrho = \pi K + \pi r, \quad K = 0, 1, \dots, \quad r \in (0, 1)$$

which separate their “large” change (by an integer multiple of the period 2π so that the trigonometric function itself remains unchanged) from a “small” change [within one period $(0, 2\pi)$]. Thus, once we define

$$\Psi = \sin 2\tau = \sin 2\pi t, \quad \Phi = \cos 2\tau = \cos 2\pi t,$$

$$\Xi = -\tan 2\varrho = -\tan \pi r,$$

all our trigonometric functions in question become independent of both the integer variables. Thus, once we decide to work, say, in the $\sigma - R$ plane, we simply introduce a lattice $\mathcal{L}_{t,r}$ of points with coordinates

$$\sigma = \sigma(N, t) = \frac{Z}{\tau(\sigma)} = \frac{Z}{\pi N + \pi t}$$

and

$$R = \frac{L - \ell}{\ell} \varrho(R) = \frac{\pi(L - \ell)}{2\ell} (K + r)$$

where $t \in (0, 1)$ and $r \in (0, 1)$ are fixed while $N = 0, 1, \dots$ and $K = 0, 1, \dots$ remain variable. Our secular equation (12) then becomes more easily analyzed at the fixed $t \in (0, 1)$ and $r \in (0, 1)$ when it may be re-read as a simplified mapping $\sigma \rightarrow R$ with

$$R = R_{t,r}(\sigma) = \Xi_r \times \frac{\sigma^4 \cosh 2\sigma + Z^2 \Phi_t}{\sigma^3 \sinh 2\sigma + \sigma Z \Psi_t}, \quad (19)$$

i.e., $R_{t,r} \approx \Xi_r |\sigma|$ at $|\sigma| \gg 1$ while

$$R_{t,r} \approx \frac{Z}{\sigma} \times \frac{\Phi_t \Xi_r}{\Psi_t}$$

at $|\sigma| \ll 1$ etc. In the subsequent step, remembering that the latter formulae hold on the lattice $\mathcal{L}(t, r)$ only, we must let this lattice move with the variation of t and/or r . Within each box numbered by the pair (N, K) of non-negative integers we would be able to re-derive all the qualitative geometric considerations of section 3 in an alternative, quantitative manner.

Appendix B: Shallow well

In the infinite-size limit $L \rightarrow \infty$ our model degenerates to a purely imaginary square well with asymptotic boundary conditions

$$\psi(\pm\infty) = 0 \quad (20)$$

and with the \mathcal{PT} symmetric matching conditions in the origin,

$$\psi(0) = 1, \quad \partial_x \psi(0) = iG. \quad (21)$$

This means that we have the general solution

$$\psi(x) = \begin{cases} \cos kx + B \sin kx, & x \in (0, \ell), & k^2 = E, \\ (L + iN) \exp(-\sigma x), & x \in (\ell, \infty), & \sigma^2 = iT^2 - k^2, \end{cases} \quad (22)$$

with $T = \sqrt{g}$ and with the the purely imaginary constant $B = iG/k$.

B.1. Matching conditions at $x = \ell$

Let us split $\sigma = p + iq$ in its real and imaginary part with $p, q \geq 0$. This gives the rules $p^2 + k^2 = q^2$ and $2pq = T^2$, easily re-parameterized in terms of a single variable α ,

$$p = q \cos \alpha, \quad k = q \sin \alpha, \quad q = \frac{T}{\sqrt{2 \cos \alpha}}, \quad \alpha \in (0, \ell/2). \quad (23)$$

The standard matching at the point of discontinuity is immediate,

$$\begin{aligned} \cos k\ell + B \sin k\ell &= (L + iN) \exp(-\sigma \ell), \\ -\sin k\ell + B \cos k\ell &= -\frac{\sigma}{k} (L + iN) \exp(-\sigma \ell). \end{aligned}$$

After we abbreviate $\sigma/k = -\tan \Omega \ell$, we get an elementary complex condition of the matching of logarithmic derivatives at $x = \ell$,

$$G = -ik \tan(k + \Omega)\ell. \quad (24)$$

Its real part defines our first unknown parameter, $G = G(\alpha)$. Due to our normalization conventions, the imaginary part of the right-hand-side expression must vanish, $\text{Re}[\tan(k + \Omega)\ell] = 0$. An elementary re-arrangement of such an equation acquires the form of an elementary quadratic algebraic equation for $X = \tan k\ell$. Its two explicit solutions read

$$X_1 = \frac{p+q}{k}, \quad X_2 = \frac{p-q}{k} \quad (25)$$

or, after all the insertions,

$$\tan \left[\frac{\ell T \sin \alpha^{(+)}}{\sqrt{2 \cos \alpha^{(+)}}} \right] = \tan \left[\frac{\ell - \alpha^{(+)}}{2} \right], \quad (26)$$

$$\tan \left[\frac{\ell T \sin \alpha^{(-)}}{\sqrt{2 \cos \alpha^{(-)}}} \right] = \tan \left[-\frac{\alpha^{(-)}}{2} \right]. \quad (27)$$

These equations specify, in implicit manner, the two respective infinite series of the appropriately bounded real roots $\alpha = \alpha_n^{(\pm)} \in (0, \ell/2)$.

B.2. Energies

For $\alpha \in (0, \ell/2)$ the left-hand-side arguments in eqs. (26) and (27) run from zero to infinity and the functions oscillate infinitely many times from minus infinity to plus infinity. In contrast, the limited variation of the argument α makes both the right-hand side functions monotonic, very smooth and bounded, $\tan[(\ell - \alpha^{(+)})/2] \in (1, \infty)$ and $\tan[\alpha^{(-)}/2] \in (0, 1)$. This indicates that our roots $k = k(\alpha_n^{(\pm)})$ will all lie within well determined intervals,

$$k_n^{(+)} \in \left(n + \frac{1}{4}, n + \frac{1}{2}\right), \quad n = 0, 1, \dots,$$

$$k_m^{(-)} \in \left(m + \frac{3}{4}, m + 1\right) \quad m = 0, 1, \dots$$

An additional merit of parametrization (23) lies in an unambiguous removal of the tangens operators from both eqs. (26) and (27). This gives

$$k_n^{(+)} = n + \frac{1}{2} - \frac{\omega_n^{(+)}}{4}, \quad k_m^{(-)} = m + 1 - \frac{\omega_m^{(-)}}{4}, \quad \omega_n^{(\pm)} = \frac{2\alpha_n^{(\pm)}}{\ell} \in (0, 1).$$

After a change of notation with $\omega_n^{(+)} = \omega_{2n}$ and $\omega_n^{(-)} = \omega_{2n+1}$, we may finally combine the latter two rules in the single secular equation

$$\sin\left(\frac{\ell}{2}\omega_N\right) = \frac{2N + 2 - \omega_N}{4T} \cdot \sqrt{2 \cos\left(\frac{\ell}{2}\omega_N\right)} \quad N = 0, 1, \dots, \quad (28)$$

In a graphical interpretation this equation represents an intersection of a tangens-like curve with the infinite family of parallel lines. This is illustrated in Figure 8. The equation generates, therefore, an infinite number of real roots $\omega_N \in (0, 1)$ at all the non-negative integers $N = 0, 1, \dots$. The discrete spectrum is unbounded from above and remains constrained by the inequalities

$$\frac{(N + 1/2)^2}{4} \leq E_N \leq \frac{(N + 1)^2}{4} \quad (29)$$

independently of the coupling T .

B.3. Wave functions

Equation (24) in combination with eqs. (26) and (27) determines the real parameter

$$G = G^{(\pm)} = -\frac{k^2}{q \pm p} \quad (30)$$

responsible for the behaviour of the wave functions near the origin [remember that $B = iG/k$ in eq. (22)]. For its deeper analysis let us first introduce an auxiliary linear function of ω and N ,

$$\sqrt{R(\omega_N, N)} = \frac{2N + 2 - \omega_N}{4T} \in \left(\frac{N + 1/2}{2T}, \frac{N + 1}{2T}\right)$$

and re-interpret our secular eq. (28) as an algebraic quadratic equation with the unique positive solution,

$$\cos\left(\frac{\ell}{2}\omega_N\right) = \frac{1}{R(\omega_N, N) + \sqrt{R^2(\omega_N, N) + 1}}. \quad (31)$$

This is an amended implicit definition of the sequence ω_N . As long as the right hand side expression is very smooth and never exceeds one, the latter formula re-verifies that the root ω_N is always real and bounded as required.

In the weak coupling regime (i.e., in the domain of the large and almost constant $R \gg 1$ with the small square-well height T or at the higher excitations), our new secular equation (31) gives a better picture of our bound-state parameters $\omega_N = 1 - \eta_N$ which all lie very close to one. The estimate

$$\frac{\ell}{2}\eta_N = \arcsin \frac{1}{R + \sqrt{R^2 + 1}} \approx \frac{1}{2R} - \frac{5}{48R^3} + \dots$$

represents also a quickly convergent iterative algorithm for the efficient numerical evaluation of the roots ω_N . One can conclude that in a way compatible with our *a priori* expectations, the value of $p = p_N = \text{Re}\sigma \approx q/2R$ is very close to zero and, as a consequence, the asymptotic decrease of our wave functions remains slow. We have $q = q_N = \text{Im}\sigma \approx k$ so that, asymptotically, our wave functions very much resemble free waves $\exp(-ikx)$. In the light of eq. (30) we have also $\psi(x) \approx \exp(-ikx)$ near the origin.

In the strong coupling regime (i.e., for very small R representing, say, the low-lying excitations in a deep well with $T \gg 1$) we get an alternative estimate

$$\frac{\ell}{4}\omega_N = \arcsin \sqrt{\frac{1}{2} \left[R - (\sqrt{1 + R^2} - 1) \right]} \approx \frac{1}{2}R - \frac{1}{4}R^2 + \dots \ll \frac{\ell}{4}.$$

In the extreme of $R \rightarrow 0$ the present spectrum of energies moves towards (and precisely coincides with) the well known levels of the infinitely deep Hermitian square well of the same width $I = (-\ell, \ell)$. In this sense, the “complex-rotation” transition from the Hermitian well to its present non-Hermitian \mathcal{PT} symmetric alternative proves amazingly smooth.

The wave functions exhibit the similar tendency. In the outer region, they are proportional to $\exp(-px)$ and decay very quickly since $p = \mathcal{O}(R^{-1/2})$. The parameter $G^{(\pm)}$ becomes strongly superscript-dependent,

$$G^{(+)} = -\frac{k^2}{q+p} = \mathcal{O}(R^{3/2}), \quad G^{(-)} = -(q+p) = \mathcal{O}(R^{-1/2}).$$

This means that in the interior domain of $x \in (-\ell, \ell)$, the wave functions with the superscript $(+)$ and $(-)$ become dominated by their spatially even and odd components $\cos kx$ and $\sin kx$, respectively. In this sense, the superscript mimics (or at least keeps the trace of) the quantum number of the slightly broken spatial parity \mathcal{P} .

Figure 1.

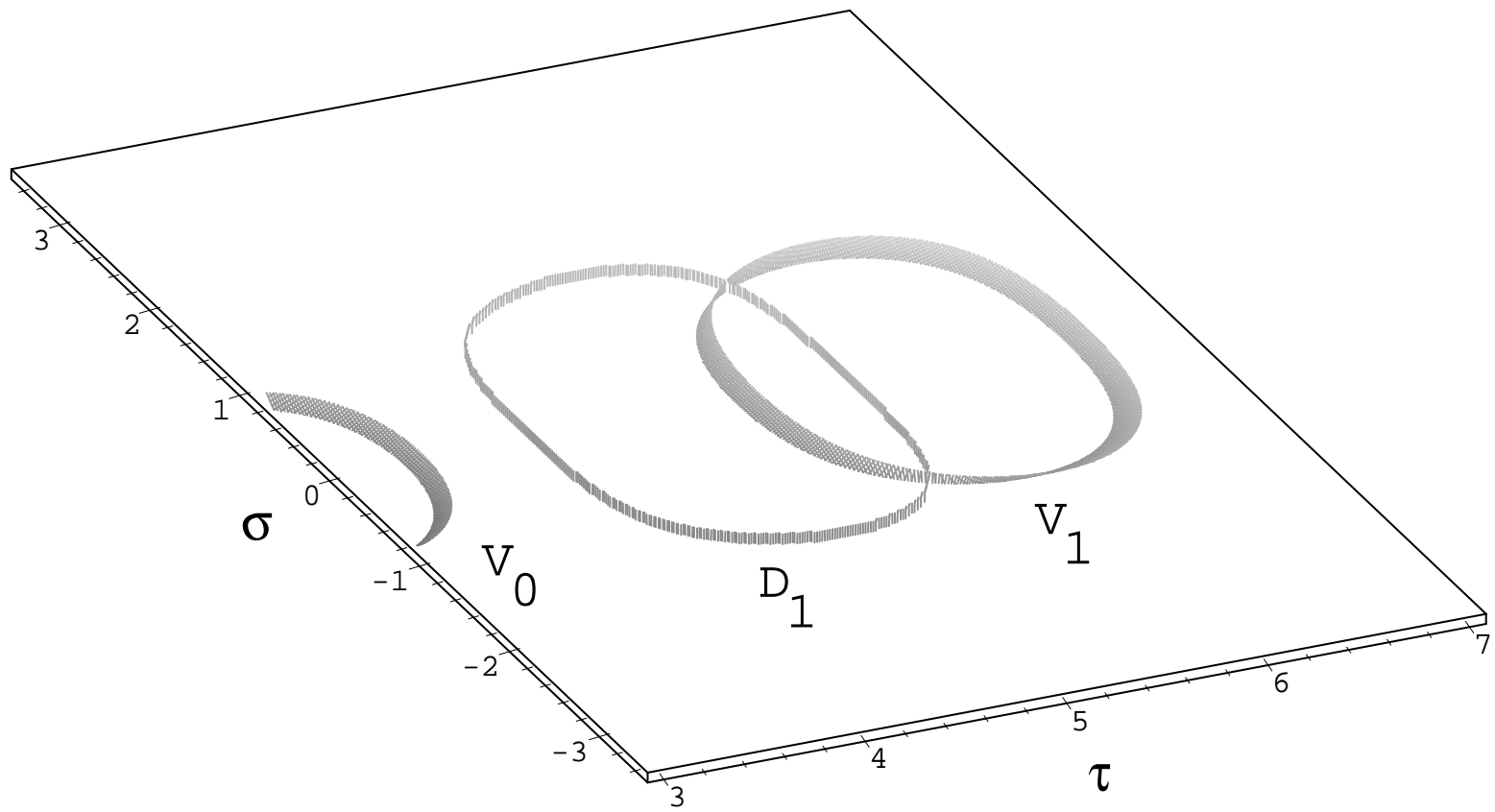


Figure 2.

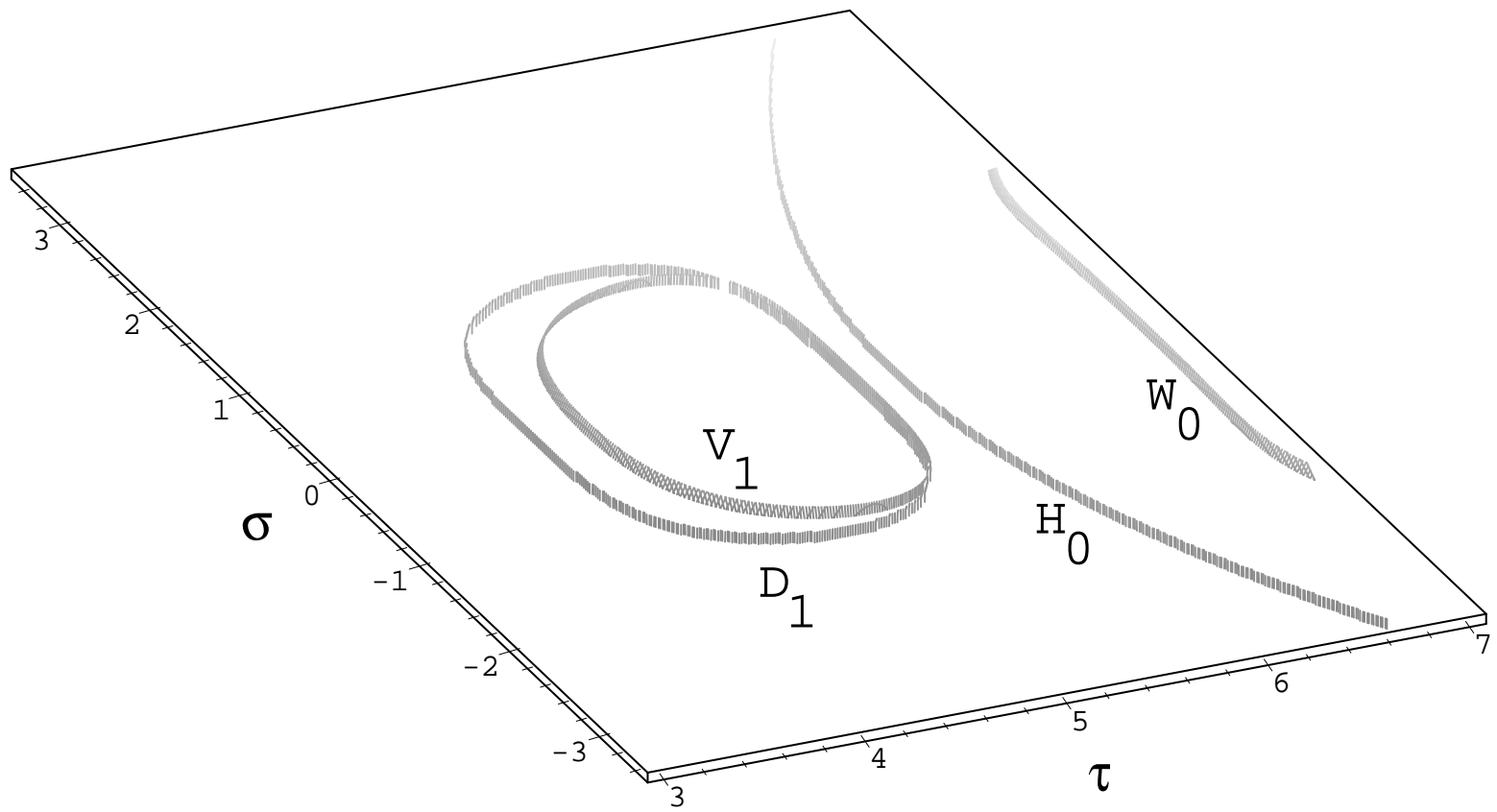


Figure 3.

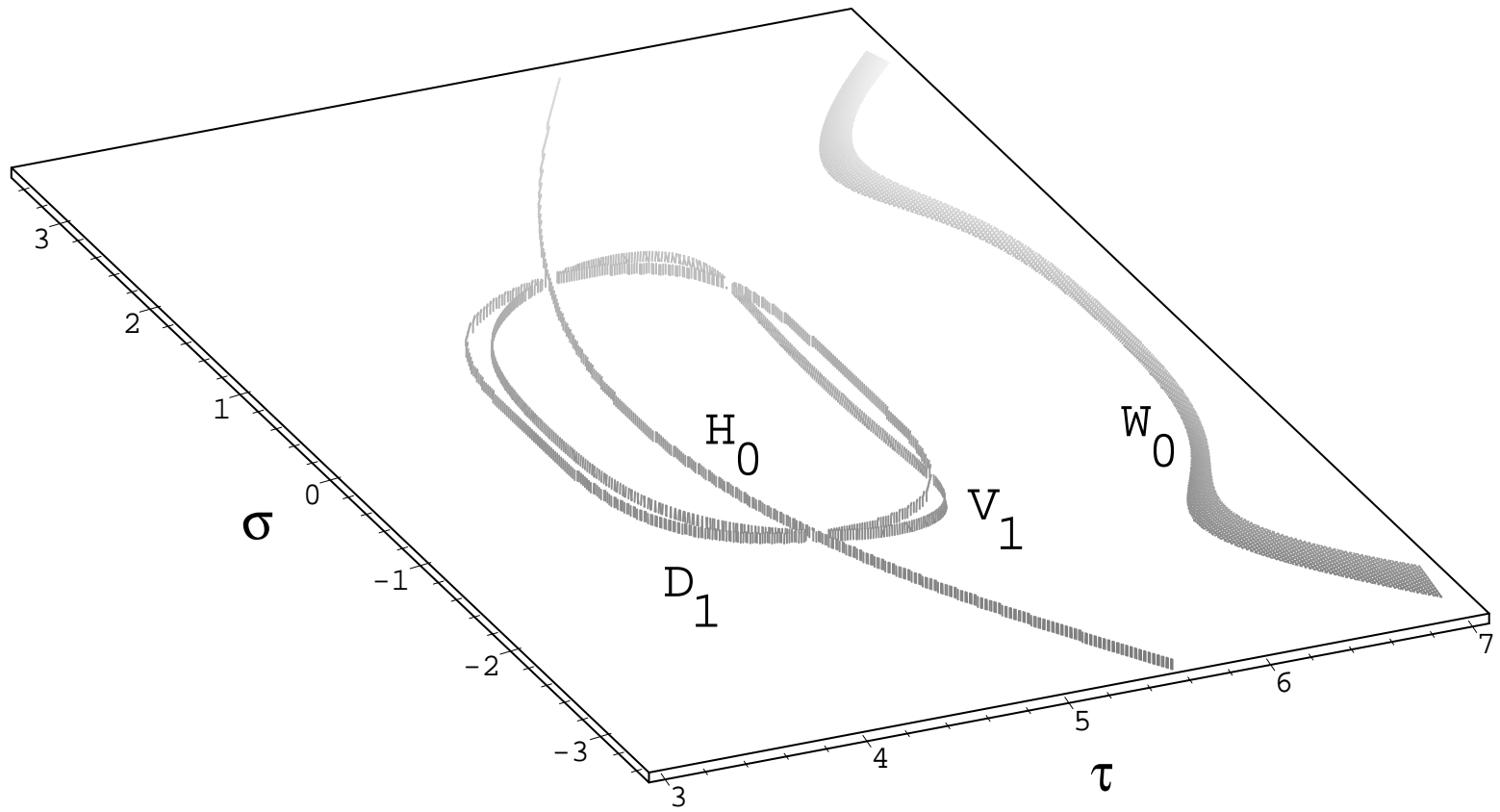


Figure 4.

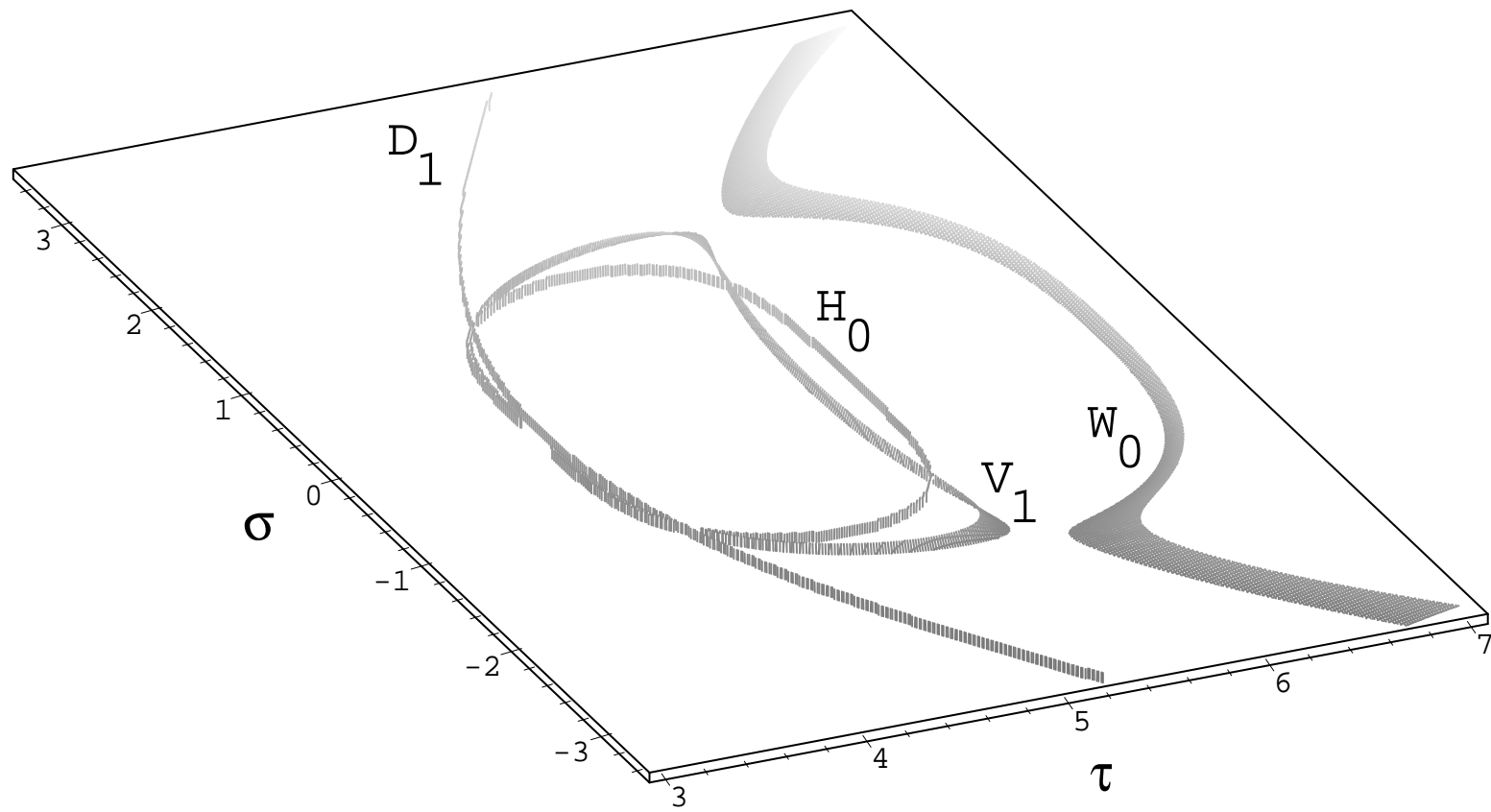


Figure 5.

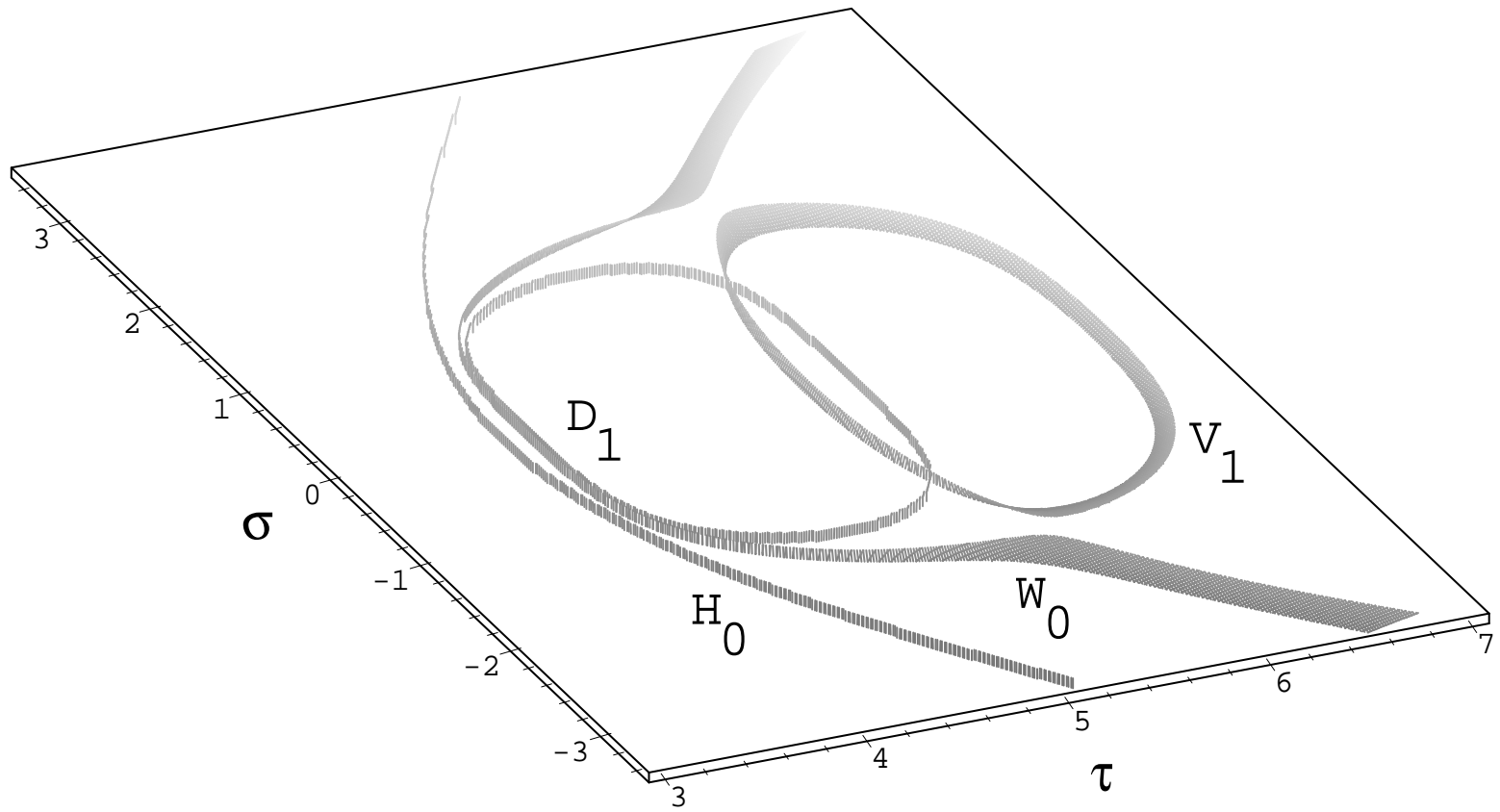


Figure 6.

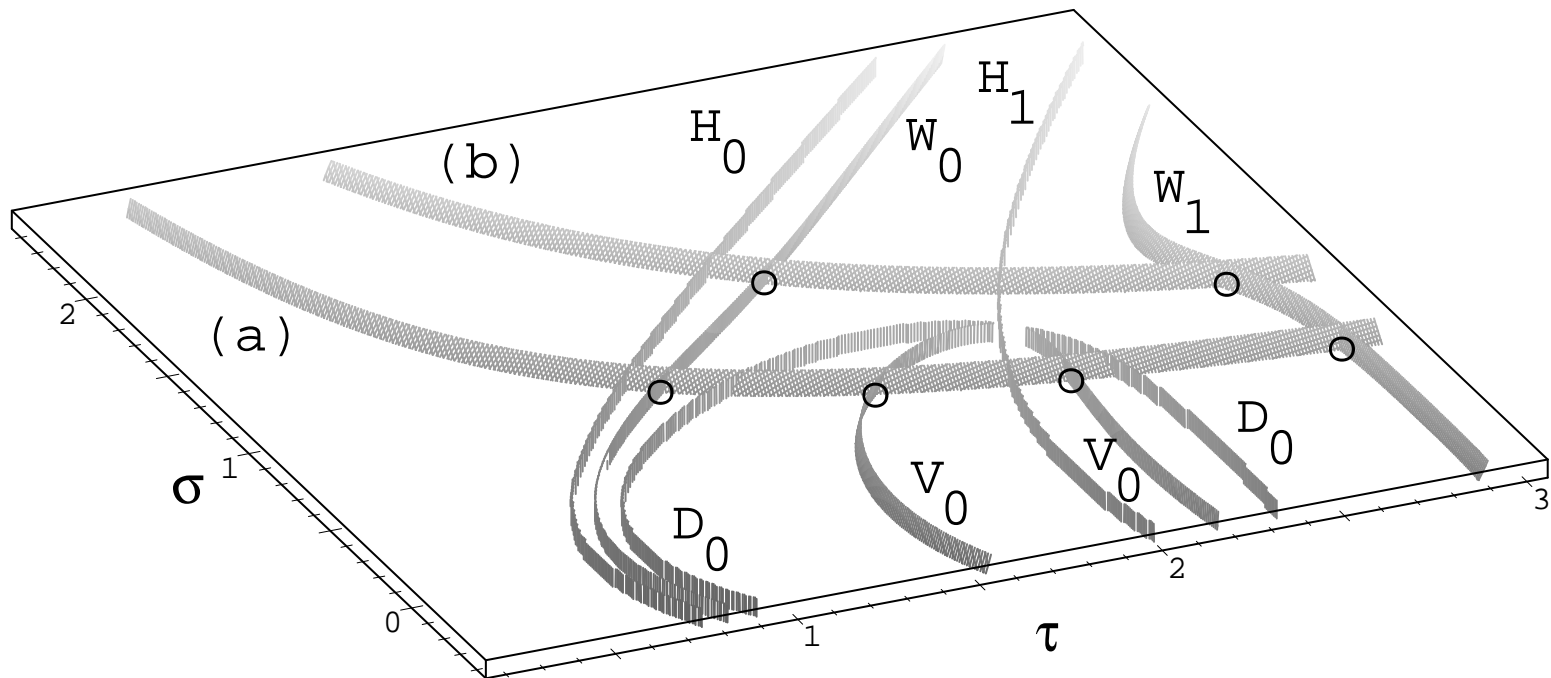


Figure 7.

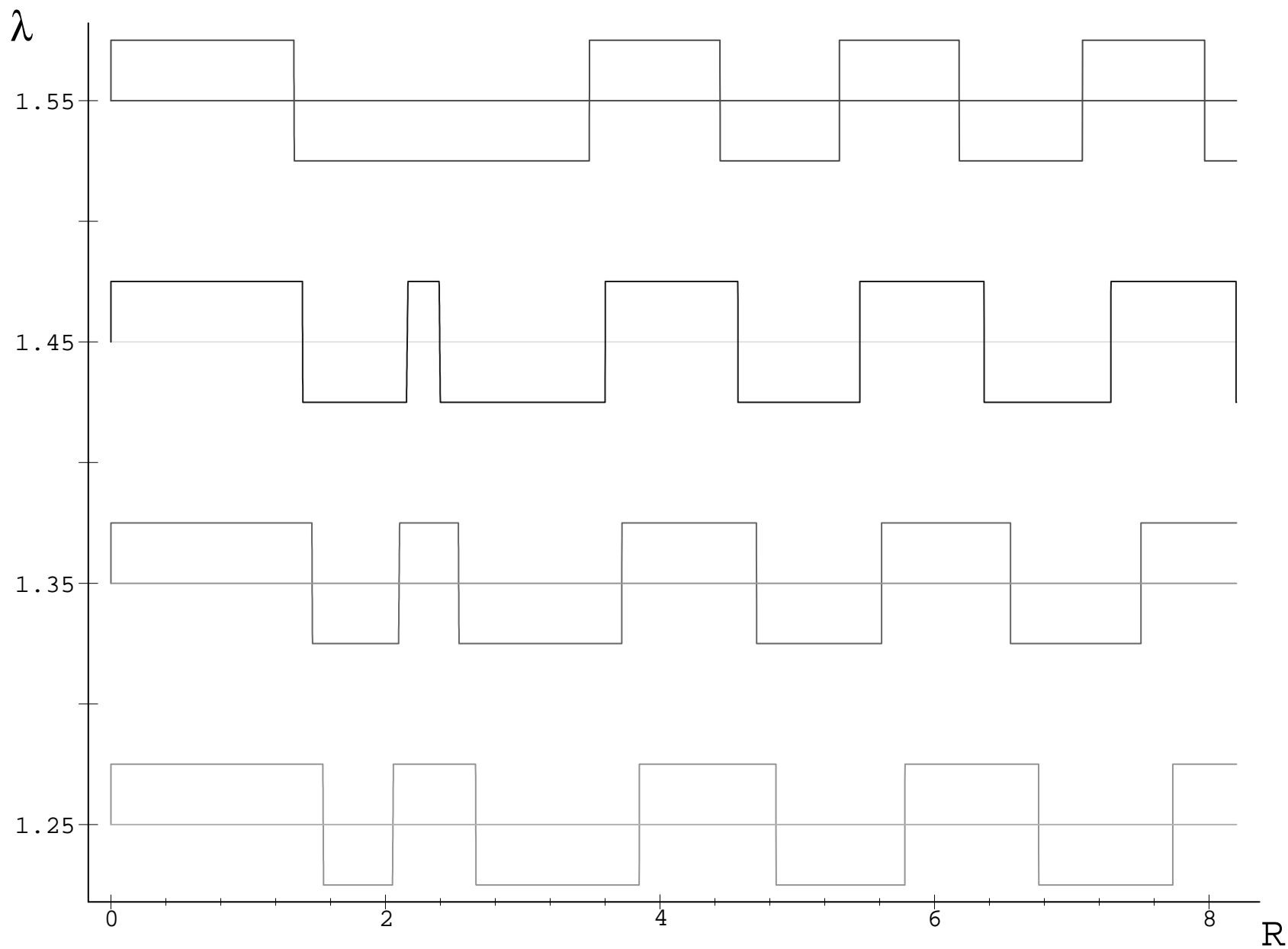


Figure 8.

